Journal of Catalysis 271 (2010) 392–400

Contents lists available at ScienceDirect

Journal of Catalysis

journal homepage: www.elsevier.com/locate/jcat

Probing the reaction intermediates for the water–gas shift over inverse CeO_x/Au(1 1 1) catalysts

Sanjaya D. Senanayake [a], Dario Stacchiola [a,b], Jaime Evans [c], Michael Estrella [a], Laura Barrio [a], Manuel Pérez [c], Jan Hrbek [a], José A. Rodriguez [a,*]

[a] The Department of Chemistry, Brookhaven National Laboratory, Upton, NY 11973, USA
[b] Department of Chemistry, Michigan Technological University, Houghton, MI, USA
[c] Facultad de Ciencias, Universidad Central de Venezuela, Caracas 1020 A, Venezuela

ARTICLE INFO

Article history:
Received 8 December 2009
Revised 30 January 2010
Accepted 22 February 2010
Available online 24 March 2010

Keywords:
Water–gas shift reaction
Ceria
Gold
CO
Water
Hydrogen
Formate
Carbonate
Photoemission
X-ray absorption fine structure

ABSTRACT

The water–gas shift (WGS) is an important reaction for the production of molecular H_2 from CO and H_2O. An inverse CeO_x/Au(1 1 1) catalyst exhibits a very good WGS activity, better than that of copper surfaces or Cu nanoparticles dispersed on a ZnO(0 0 0 $\bar{1}$) substrate which model current WGS industrial catalysts. In this work we report on intermediates likely to arise during the CO + H_2O reaction over CeO_x/Au(1 1 1) using soft X-ray photoemission (sXPS) and near-edge X-ray absorption fine structure (NEXAFS). Several potential intermediates including formates (HCOO), carbonates (CO_3) and carboxylates (HOCO) are considered. Adsorption of HCOOH and CO_2 is used to create both HCOO and CO_3 on the CeO_x/Au(1 1 1) surface, respectively. HCOO appears to have greater stability with desorption temperatures up to 600 K while CO_3 only survives on the surface up to 300 K. On the CeO_x/Au(1 1 1) catalysts, the presence of Ce^{3+} leads to the dissociation of H_2O to give OH groups. We demonstrate experimentally that the OH species are stable on the surface up to 600 K and interact with CO to yield weakly bound intermediates. When there is an abundance of Ce^{4+}, the OH concentration is diminished and the likely intermediates are carbonates. As the surface defects are increased and the Ce^{3+}/Ce^{4+} ratio grows, the OH concentration also grows and both carbonate and formate species are observed on the surface after dosing CO to H_2O/CeO_x/Au(1 1 1). The addition of ceria nanoparticles to Au(1 1 1) is essential to generate an active WGS catalyst and to increase the production and stability of key reaction intermediates (OH, HCOO and CO_3).

1. Introduction

The production of H_2 has become an important issue in the pursuit of energy sources derived from reliable and sustainable resources [1]. Currently, most methods of H_2 production require its separation from 'carbon and hydrogen containing' feedstocks using chemical and thermal processes (biological methods remain exploratory) including reactions such as steam reforming of natural gas (1) or ethanol (2) [1–3].

$$CH_4 + H_2O \rightarrow CO + 3H_2 \quad (1)$$
$$CO + H_2O \longleftrightarrow H_2 + CO_2$$
$$CH_3CH_2OH + H_2O \rightarrow 2CO + CH_4 + H_2 \quad (2)$$
$$CO + H_2O \longleftrightarrow H_2 + CO_2$$
$$CH_4 + 2H_2O \rightarrow 4H_2 + CO_2$$

In both of the above cases the water–gas shift (WGS) reaction (CO + $H_2O \longleftrightarrow H_2 + CO_2$) is a critical step in the production of additional H_2 and the conversion of poisonous CO to CO_2 [1,2]. Ceria (CeO_x)-containing materials are involved in many reactions as catalysts [2,3]. The Au–CeO_2 system is an excellent catalyst for the WGS reaction [2]. It has some advantages over the traditional Cu/ZnO catalysts which are usually pyrophoric materials and deactivate during redox and condensation steps. In this study we investigate the behavior and properties of an inverse CeO_x/Au(1 1 1) catalyst that exhibits a WGS activity greater than those of copper surfaces [4]. As shown in Scheme 1, an inverse oxide/metal catalyst exposes oxide nanoparticles to the reactants. Defect sites present in the oxide are not covered by metal particles, as in the case of a traditional metal/oxide catalyst [2–4]. In the inverse catalyst, the reactants can interact with defect sites of ceria nanoparticles, metal sites of the support, or the metal–oxide interface [4]. One can gain activity due to the active participation of oxide in the catalytic reaction [4].

Ceria is a reducible oxide that has unique oxygen storage properties that allow an interchangeable set of oxidation states ($Ce^{3+} \longleftrightarrow Ce^{4+}$). It can accommodate a large number of oxygen vacancies and hence participates readily in many redox reactions [2–4]. Au(1 1 1) displays no activity for H_2O dissociation and

* Corresponding author. Fax: +1 631 344 5815.
E-mail address: rodrigez@bnl.gov (J.A. Rodriguez).

0021-9517/$ - see front matter © 2010 Elsevier Inc. All rights reserved.
doi:10.1016/j.jcat.2010.02.024

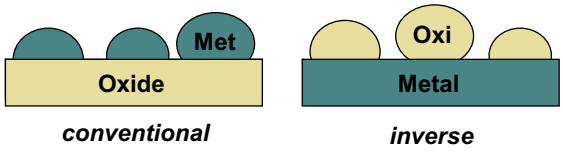

Scheme 1.

production of OH except in the presence of chemisorbed O [5]. Bulk CeO_2(1 1 1) has no reported activity toward the WGS but does have the ability to dissociate H_2O in the presence Ce^{3+} [6] as is commonly the case in reducible oxides (TiO_x, MoO_x). However, when a small concentration of CeO_x nanoparticles is in contact with the Au(1 1 1) surface, there is significant activity toward the WGS [4].

Post-reaction characterization of the inverse CeO_x/Au(1 1 1) catalyst with X-ray photoelectron spectroscopy (XPS) identified a C1s feature at 289–290 eV corresponding to either HCOO or CO_3 species on the CeO_x/Au(1 1 1) surface [4]. The mechanism for the WGS in CeO_x/Au(1 1 1) was assumed to undergo the following pathway:

$$CO \rightarrow CO\ (a)$$
$$H_2O \rightarrow H_2O\ (a)$$
$$H_2O\ (a) \rightarrow OH\ (a) + H\ (a)$$
$$CO\ (a) + OH\ (a) \rightarrow HCO_x\ (a)$$
$$HCO_x\ (a) \rightarrow CO_2 + H\ (a)$$
$$2H\ (a) \rightarrow H_2$$

A stable HCO_x intermediate species must precede the formation of H_2 and CO_2. It has been proposed but not generally accepted that the predominant intermediate species for this reaction is either a *formate* (HCOO) [7] or a *carbonate* (CO_3) [8] (see Scheme 2). Recent theoretical calculations also suggest the possibility of a *carboxylate* (HOCO) intermediate [4].

In the past, we have explored the stability of formates, carbonates, and the reaction of CO and OH over oxygenated Au(1 1 1) surfaces [5]. The clean Au(1 1 1) surface was inactive for the formation of HCOO or CO_3 but in the presence of chemisorbed atomic O (0.2 ML) we were able to observe both species with formate being the more strongly bound surface intermediate. OH also readily formed from the dissociation of H_2O and showed a weak interaction with CO bound on O/Au(1 1 1). The $OH + CO \rightarrow CO_2 + 0.5H_2$ reaction takes place on O/Au(1 1 1) at very low temperature (80–120 K) [9]. The OH + CO interaction did not show experimental evidence for the formation of either a carbonate or a formate intermediate species. It was hence postulated that a carboxylate species could be a probable intermediate. This species is likely to have a short surface lifetime (during the OH + CO reaction) while the formation of either formate or carbonate intermediates would lead to surface poisoning as active sites responsible for the dissociation of H_2O would be blocked and continued reactivity prevented.

In this article, we investigate the WGS reaction on an inverse CeO_x/Au(1 1 1) catalyst at temperatures between 573 and 650 K.

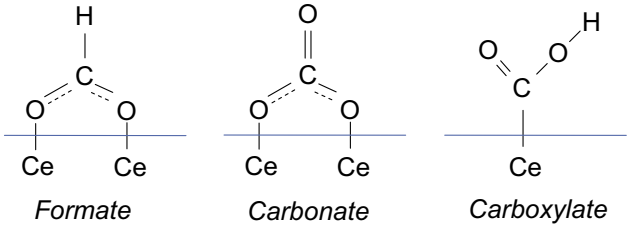

Scheme 2.

XPS and near-edge X-ray absorption fine structure (NEXAFS) are used to characterize the formate and carbonate intermediates that form on the CeO_x/Au(1 1 1) surface and probe the intermediate that arises during the $CO + OH \rightarrow CO_2 + 0.5H_2$ reaction. Although formates and carbonates are essentially indistinguishable in XPS, they can be identified by NEXAFS measurements at the C K - edge [5,10].

2. Experimental

Part of the experiments were carried out in an ultrahigh-vacuum (UHV) chamber that has attached a high-pressure cell or batch reactor [4]. The sample could be transferred between the reactor and UHV chamber without exposure to air. The UHV chamber (base pressure $\sim 1 \times 10^{-10}$ Torr) was equipped with instrumentation for XPS, low-energy electron diffraction (LEED), ion-scattering spectroscopy (ISS), and thermal-desorption mass spectroscopy (TDS) [4]. The photoemission and NEXAFS experiments performed in this study were undertaken in an UHV endstation at beamline U12A of the National Synchrotron Light Source (NSLS) in Upton, New York. Sample growth and adsorbate characterization were conducted with *in situ* soft X-ray photoemission (sXPS) and NEXAFS measurements using synchrotron radiation introduced into the chamber. The sXPS C1s and O1s regions were excited at 400 eV and 650 eV photon energy with a resolution of 0.2 eV and 0.3 eV, respectively. The NEXAFS was undertaken using a partial yield detector (PYD) with a grid biased at 225 eV (C K - edge). Angle-resolved measurements with NEXAFS were restricted to a normal incidence (0°) and grazing incidence (65°) angles. The photon energy calibration was undertaken for the XPS and NEXAFS measurements with alignment to the Ce 4d satellite peak at 122.3 eV and to the dip in the photon flux at 284.7 eV, respectively.

CeO_x was grown *in situ* onto the gold substrate (1×10^{-7} Torr of O_2 at 700 K, followed by annealing to 900 K), and the CeO_x/Au(1 1 1) system has been extensively characterized previously with XPS [11] and scanning tunneling microscopy (STM) [12]. In this study the films were grown with the use of an e-beam evaporator at an evaporation rate of ~0.03 monolayer (ML)/min. The 'as-grown' films are represented as CeO_x that denotes a surface that is almost fully oxidized: $CeO_{1.95-1.98}$. In experiments when a well-oxidized surface was required, the films were annealed in O_2 (1×10^{-6} Torr) for 30 min at 800 K to maximize the Ce^{4+} concentration and are subsequently denoted as CeO_2. Reduced surfaces were obtained by annealing the as-grown surfaces in ethanol (1×10^{-6} Torr) at 600 K, followed by annealing to 900 K to remove any residual hydrocarbon, and these surfaces are labeled $CeO_{1.75}$/Au(1 1 1). Both the well-oxidized and reduced surfaces were characterized with Ce 3d or 4d XPS, and the relative concentrations of Ce^{3+} to Ce^{4+} were thus established [4].

In the tests of WGS activity, done in the UHV chamber which has attached a batch reactor [4], the sample was transferred to the reactor at ~300 K, then the reactant gases were introduced (20 Torr of CO and 10 Torr of H_2O) and the sample was rapidly heated to the reaction temperature (573, 600, 625 or 650 K). Product yields were analyzed by a gas chromatograph [13]. The amount of molecules produced was normalized by the active area exposed by the front of the sample. The sample holder was passivated by extensive sulfur poisoning (exposure to H_2S) and has no catalytic activity [4]. XPS spectra showed that there was no migration of S from the sample holder to the oxide/gold surfaces. In our batch reactor, a steady-state regime for the production of H_2 and CO_2 was reached after 1–2 min of reaction time. The kinetics experiments were done in the limit of low conversion (<5%).

Possible intermediates in the WGS were generated by adsorption of formic acid, water, CO and CO_2 on the CeO_x/Au(1 1 1)

surfaces. Formic acid was obtained from Sigma Aldrich at a purity of 99% and contained in a stainless steel bulb. CO_2 and CO were obtained from Matheson Trigas and had a purity of 99.99%. H_2O was obtained from a Millipore source located in-house. Both formic acid and H_2O were purified with several cycles of freeze–pump–thaw using liquid N_2. All adsorbates were checked for purity with mass spectrum analysis using a residual gas analyzer (RGA).

3. Results

3.1. Water–gas shift activity of inverse CeO_x/Au(1 1 1) catalysts

The clean Au(1 1 1) surface is inactive as a catalyst for the WGS reaction. This surface does not bind water well and is not able to dissociate O–H bonds [4,14]. The addition of ceria nanoparticles to Au(1 1 1) produces an excellent catalyst for the WGS. In a previous work the WGS was investigated on CeO_x/Au(1 1 1) surfaces at a temperature of 573 K under a CO pressure of 20 Torr and a water pressure of 10 Torr [4]. The fraction of the gold substrate covered by ceria was measured by ISS and was varied from 0 to 1, with the maximum of catalytic activity found at a fractional ceria coverage of 0.2 [4]. At this coverage, the reactants can interact with defect sites of the supported ceria nanoparticles, sites of the gold substrate, or the metal–oxide interface [4]. Here, we performed similar type of studies at temperatures of 600, 625, and 650 K. In Fig. 1, we display an Arrhenius plot for the WGS activity of a CeO_x/Au(1 1 1) surface in which 20% of the gold substrate was covered by ceria. For comparison we also include results obtained for the WGS on Cu(1 0 0) [15], Cu(1 1 1) [16] and Cu/ZnO(0 0 0 $\bar{1}$) [17] surfaces. Cu is the best-known metal catalyst for the WGS [14,17]. The results in Fig. 1 indicate that the inverse CeO_x/Au(1 1 1) catalyst exhibits a larger WGS activity than those of copper surfaces or even Cu nanoparticles dispersed on a ZnO(0 0 0 $\bar{1}$) substrate. On Cu(1 1 1) and Cu(1 0 0), the apparent activation energies for the WGS are 18.1 and 15.2 kcal/mol, respectively [15,16]. The apparent activation energy decreases to 12.4 kcal/mol on Cu/ZnO(0 0 0 $\bar{1}$) [15] and 10.3 kcal/mol on CeO_x/Au(1 1 1).

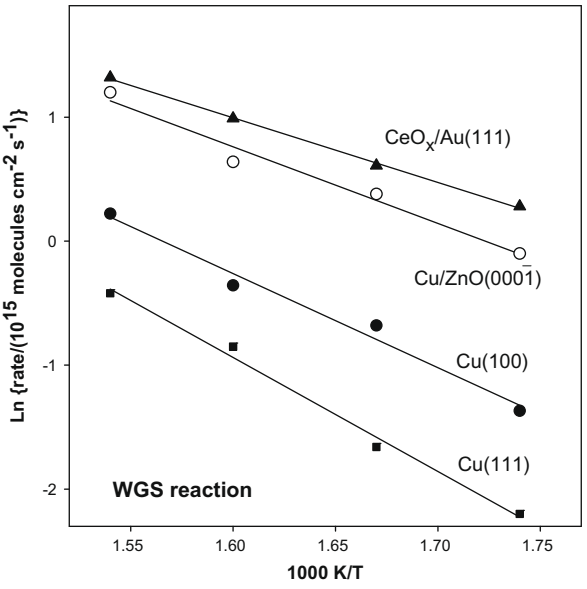

Fig. 1. Arrhenius plot for the WGS reaction rate on Cu(1 1 1), Cu(1 0 0), Cu/ZnO(0 0 0 $\bar{1}$), and on a Au(1 1 1) surface approximately 20% covered by ceria. The CeO_x/Au(1 1 1) surface was prepared as described in Section 2, and before the reaction the oxide nanoparticles had a composition close to CeO_2. The data were acquired with a pressure of 20 Torr of CO and 10 Torr of H_2O. The results for Cu(1 1 1), Cu(1 0 0), and Cu/ZnO(0 0 0 $\bar{1}$) were taken from Refs. [15,16].

After collecting the kinetic data in Fig. 1, the gases were pumped out from the reaction cell and the CeO_x/Au(1 1 1) surface was post-characterized using XPS. The XPS showed a small signal for adsorbed CO_x groups with a C1s binding energy of 289.6–289.9 eV. This binding energy matches well with those found for formate (HCOO) and carbonate (CO_3) groups bonded to CeO_x/Au(1 1 1), as we will discuss below. The XPS data also indicated a lack of oxidation of the Au substrate. The catalysts exhibited Au 4f spectra that were practically identical to those of Au(1 1 1) and very different from those expected for AuO_x species or Au incorporated into the ceria lattice [18]. The lack of oxidation of the Au substrate seen in the XPS data are consistent with *in situ* measurements of X-ray absorption spectroscopy for high-surface area catalysts [18,19], which show that $Au^{\delta+}$ species are not stable under typical WGS conditions. In the Ce 3d XPS spectra of CeO_x/Au(1 1 1), there was a decrease in the amount of Ce^{4+} present in the sample during the WGS. An analysis of the lineshape for the Ce 3d spectra [4] pointed to a composition of $\sim CeO_{1.7}$ after the WGS reaction showing reduction from an initial $CeO_{1.95–1.98}$ composition.

3.2. Formates (HCOO) on CeO_x/Au(1 1 1)

Clean Au(1 1 1) does not react with formic acid [5]. The reactivity of HCOOH on a CeO_2(1 1 1) single-crystal and on CeO_2(1 0 0) and CeO_2(1 1 1) films was previously studied by Stubenrauch et al. [20] and Senanayake et al. [10]. The presence of adsorbed formate was detected, with a substantial difference in stability and bonding mode (monodentate vs. bidentate coordination) depending on the concentration of defects on the ceria surfaces [10,20]. On the CeO_2(1 1 1) single-crystal, formate was stable up to $\sim$610 K, decomposing primarily into CO and H_2O with small amounts of CO_2 and H_2CO [20]. For the adsorption of HCOOH on ceria films grown on Ru(0 0 0 1), the formation of formates and carbonates (from CO_2 adsorption) was reported using XPS and NEXAFS on both oxidized (CeO_2(1 1 1)) and reduced ($CeO_{1.75}$(1 1 1)) surfaces [10]. On a CeO_2(1 1 1) film, it was observed that formates remained on the surface up to 560 K and C K - edge NEXAFS measurements were required to distinguish the species from carbonates. Fig. 2 shows C1s and O1s spectra collected after dosing 12 L of formic acid (HCOOH) on to a cool (100 K) CeO_x/Au(1 1 1) surface. In the C1s region, a single peak at 291 eV appears that corresponds to molecularly bound ice layers of formic acid as observed previously on Au(1 1 1) [5] and CeO_2 [10] surfaces. Annealing to 200 K shows a shift and broadening of the peak to $\sim$289 eV. A broad lineshape suggests the presence of two species with peaks visible at this stage at 289 and 289.5 eV. These can be matched to physisorbed HCOOH on both Au(1 1 1) [5] and CeO_2(1 1 1) [10] surfaces. A small broad feature at 286.5 eV is also evident that is not observed on the clean CeO_x/Au(1 1 1) surface. The position of this peak may correspond to a potential C–O species [5]. At 300 K, this peak is more prominent but the 289.5 eV peak has also disappeared leaving just the feature at 289 eV. On the Au(1 1 1) surface, the physisorbed HCOOH is reported to desorb below 300 K [5] but on CeO_2(1 1 1) a formate is the likely intermediate [10]. So hence the 289 eV peak most likely arises from the dissociation of the acid proton of HCOOH to give HCOO bound to CeO_x. This species remains stable between 300 and 400 K but decomposes beyond 400 K. At 500 K, the 289 eV peak appears shifted to 289.5 eV and the 286.5 eV peak appears more prominent. By 600 K, only traces of a C species are left on the surface and all the HCOO and C–O species have desorbed.

Fig. 2B corresponds to the same experiment described in Fig. 2A but shows the O1s region. At 100 K, the 12 L exposure of HCOOH gives rise to a single O peak at 535 eV. The lattice O species has been buried under formic acid ice formed on the surface. Annealing

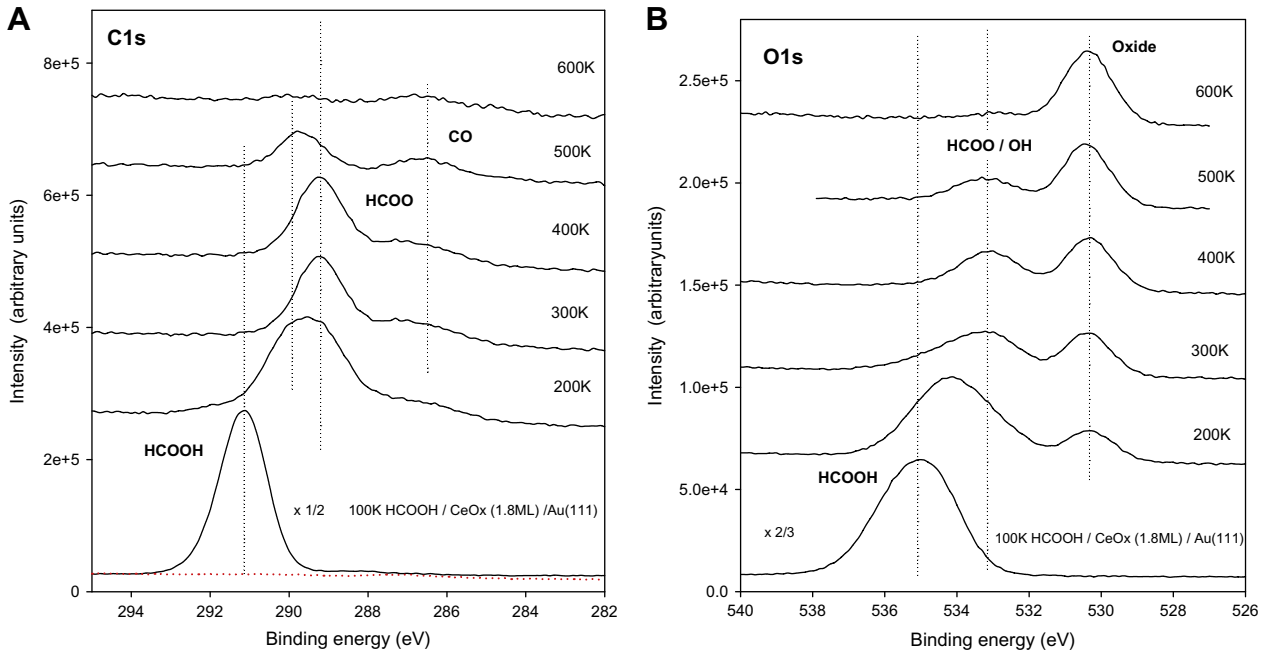

Fig. 2. (A) Soft X-ray photoelectron spectra (sXPS) for the C1s region upon 12 L of HCOOH dosed onto a CeO_x/Au(1 1 1) surface at 100 K followed by subsequent heating from 100 to 600 K. The corresponding spectra for clean CeO_x/Au(1 1 1) are shown as dotted traces. (B) O1s spectra for the adsorption of HCOOH (12 L) on CeO_x/Au(1 1 1) at 100 K, followed by annealing steps up to 600 K. The corresponding C1s spectrum for clean CeO_x/Au(1 1 1) is shown as dotted traces.

to 200 K causes the 535 eV peak to broaden as the multilayer of HCOOH desorbs and we see the appearance of the lattice O (CeO_x) peak at 530.2 eV. By 300 K, the HCOO can be distinguished from HCOOH with a single peak at 533.2 eV alongside a stronger 530.2 eV lattice peak. Continued heating induces desorption of the intermediate (533.2 eV) and the re-appearance of the lattice species (530.2 eV) around 600 K when the only O1s present is from the CeO_x.

The pathways for decomposition of HCOOH and HCOO may occur as follows:

$$\mathrm{HCOOH} + \mathrm{O\ (oxide)} \rightarrow \mathrm{HCOO\ (a)} + \mathrm{OH\ (a)}$$
$$\mathrm{2OH\ (a)} \rightarrow \mathrm{H_2O} + \mathrm{O\ (oxide)}, \quad \sim 300\ \mathrm{K}\ [10]$$
$$\mathrm{2HCOO\ (a)} \rightarrow \mathrm{2CO\ (a)} + \mathrm{H_2O} + \mathrm{O\ (oxide)}, \quad \sim 300\ \mathrm{K}$$
$$\mathrm{2HCOO\ (a)} \rightarrow \mathrm{2CO_2} + \mathrm{H_2}, \quad \sim 360\ \mathrm{K}\ [10]$$
$$\mathrm{CO\ (a)} \rightarrow \mathrm{CO}, \quad 450\text{–}600\ \mathrm{K}$$
$$\mathrm{HCOO\ (a)} \rightarrow \mathrm{CO} + 1/2\mathrm{H_2} + \mathrm{O\ (oxide)}, \quad 450\text{–}600\ \mathrm{K}\ [10]$$

The HCOO species formed on the ceria nanoparticles supported on Au(1 1 1) appear to decompose at lower temperatures than formate species bonded to a CeO_2(1 1 1) single-crystal [20] or a CeO_2(1 1 1) film [10]. This difference in stability makes formate a possible intermediate for the WGS reaction on CeO_x/Au(1 1 1) and highlights the advantage of having oxide nanoparticles in an inverse oxide/metal catalyst.

Fig. 3 shows C K - edge NEXAFS data following the adsorption of HCOOH (12 L) and annealing to 300 K at 0° and 65° incidence angles. The main peaks observed are at are at 288, 290.6, 299.4 and 301.7 eV corresponding to the π^*C=O, σ^*CH, σ_1^*CO and σ_2^*C=O resonances, respectively. The π^*C=O and σ_2^*C=O resonances favor the normal (0°) incidence while the σ^*CH and σ_1^*CO the grazing incidence (65°). These spectra are in good agreement with those observed for formates on O/Au(1 1 1) [5] and CeO_2(1 1 1) films [10]. The orientation of the formate on the ceria nanoparticles supported on Au(1 1 1) is likely to be near normal to the surface as a bidentate species in a chelating or bridged conformation [5,10], which is in contrast to the mondentate species reported by

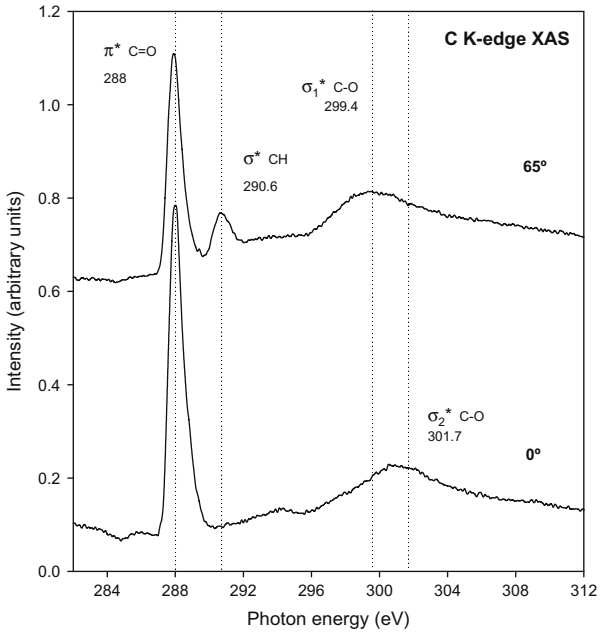

Fig. 3. C K - edge NEXAFS of HCOOH adsorbed onto CeO_x/Au(1 1 1) at 100 K and annealed to 300 K. Both the normal incidence (0°) angle and the grazing incidence (65°) spectra are presented here.

Stubenrauch et al. on a CeO_2(1 1 1) single-crystal surface [20]. Thus, when going from bulk CeO_2(1 1 1) to CeO_x/Au(1 1 1), there is a difference in the stability and bonding geometry of formate.

3.3. Carbonates (CO_3) on CeO_x/Au(1 1 1)

CO_2 only physisorbs on a clean Au(1 1 1) surface [5]. The molecule interacts better with O/Au(1 1 1) forming a carbonate that decomposes by 150 K [5]. Fig. 4 shows C1s spectra collected upon

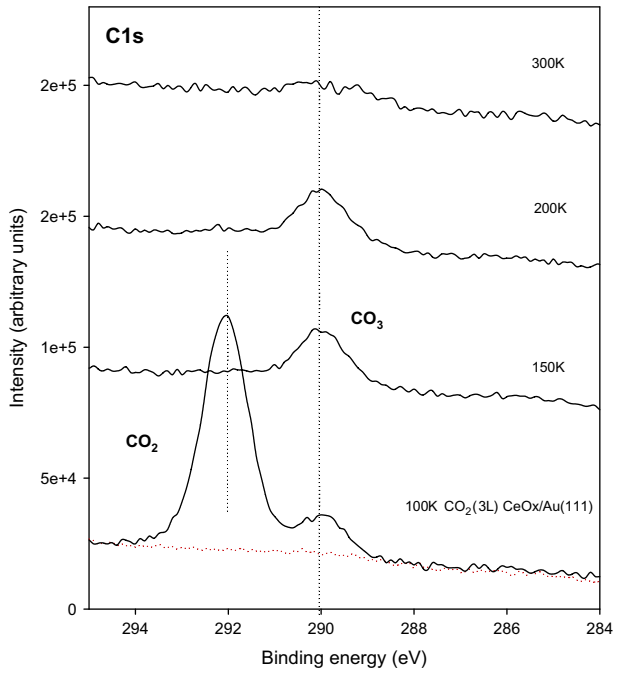

Fig. 4. Soft X-ray photoelectron spectra (sXPS) of the C1s region upon a 3 L dose of CO_2 to a CeO_x/Au(1 1 1) surface at 100 K followed by subsequent heating from 100 to 300 K. The corresponding spectrum for clean CeO_x/Au(1 1 1) is shown as dotted traces.

an exposure of 3 L of CO_2 to a CeO_x/Au(1 1 1) surface at 100 K. Two peaks at 292 and 290 eV appear at initial adsorption and can be correlated to multilayers of physisorbed CO_2 and chemisorbed CO_3, respectively [10]. Annealing to 150 K causes the physisorbed CO_2 to desorb leaving only CO_3 on the surface. This intermediate is stable and after annealing to 300 K all the C species desorbs from the surface. In comparison with the adsorbed formate, the desorption temperature of the carbonate is much lower and indicates weaker binding to the surface. However, compared to the O/Au(1 1 1) surface [5] this carbonate species is bound a lot stronger. For the carbonate species on O/Au(1 1 1), decomposition is observed at temperatures below 150 K.

Fig. 5 shows the same experiment in the O1s region. The lattice O peak from CeO_x is present in all spectra at 530.2 eV with varying degrees of intensity depending on the desorption of the intermediate. At 100 K, with an exposure of 3 L of CO_2 a peak at 535.9 eV appears with traces of a shoulder at 532 eV. This 535.9 eV is the contribution from the multilayers of CO_2. With annealing to 150 K this peak has disappeared leaving two features at 533.5 and 532 eV. Annealing between 150 and 200 K shows the same stable pair of species but by 300 K only the 532 eV peak remains. The 533.5 eV peak is likely to be a contribution from the CO_3 species that desorbed by 300 K while the 532 eV could be O contribution from a noncarbon containing intermediate such as OH or weakly bound surface O.

Based on both the O1s and C1s spectra, it is possible to conclude that the reaction pathway of CO_2 on CeO_x/Au(1 1 1) may follow the sequence:

$$2CO_2 + O\ (\text{oxide}) \rightarrow CO_2\ (a) + CO_3\ (a), \quad \sim 100\ \text{K}\ [10]$$
$$CO_2\ (a) \rightarrow CO_2, \quad \sim 150\ \text{K}$$
$$CO_3\ (a) \rightarrow CO_2 + O\ (\text{oxide}), \quad \sim 300\ \text{K}$$

Fig. 6 shows the C K - edge NEXAFS spectra of 3 L of CO_2 adsorbed onto the CeO_x/Au(1 1 1) surface followed by annealing to 170 K. The main peak with no distinct preference appears equally in both the normal and the grazing incidence at 289.1 eV corresponding to a π^*C–O resonance. Weaker contributions are also observed at 285.9, 289.3, and 300.2 eV. The 289.3 and 300.2 eV contributions are likely to be σ_1^*C–O features that appear in the normal and grazing incidence, respectively. The 285.9 eV could likely be traces of CO species that arise from contaminants or beam damage [5] although there is no evidence of beam damage observed in the sXPS data described above. The CO_3 species observed on the inverse CeO_x/Au(1 1 1) catalysts decompose at a temperature (~300 K) considerably lower than that

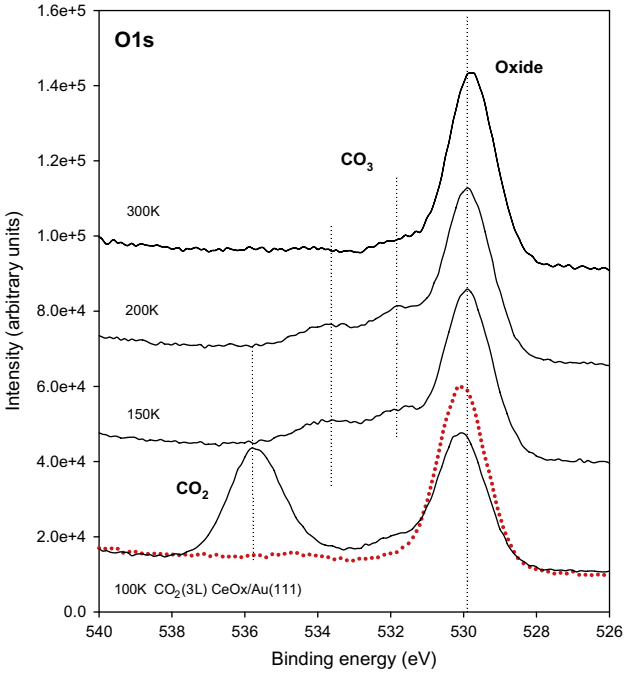

Fig. 5. O1s spectra for the adsorption of CO_2 (12 L) on CeO_x/Au(1 1 1) at 100 K, followed by annealing steps up to 300 K. The corresponding spectrum for clean CeO_x/Au(1 1 1) is shown as dotted traces.

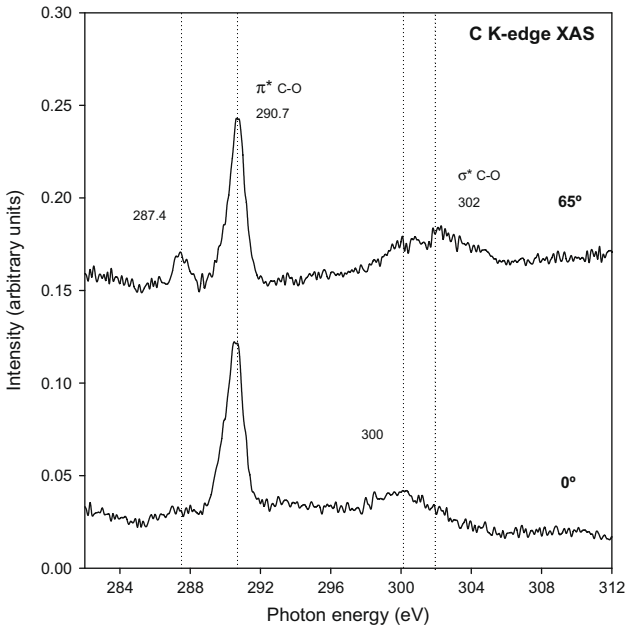

Fig. 6. C K - edge NEXAFS spectra for the adsorption of CO_2 on CeO_x/Au(1 1 1) at 100 K and annealing to 300 K. Both the normal incidence (0°) angle and the grazing incidence (65°) spectra are presented here.

seen for the decomposition of CO_3 species bonded to high-surface area M/CeO_2 catalysts (~600 K) [8]. As in the case of adsorbed formate, the difference in stability for carbonate on bulk ceria and on the ceria nanoparticles makes the carbonate a possible intermediate for the WGS reaction on $CeO_x/Au(1\,1\,1)$, and also highlights the advantage of having oxide nanoparticles in an inverse oxide/metal catalyst.

3.4. Hydroxyls (OH) on $CeO_x/Au(1\,1\,1)$

H_2O dissociation was investigated on $CeO_2(1\,1\,1)$ films [6] and on $CeO_x/Au(1\,1\,1)$ surfaces [21], with spectroscopic evidence demonstrating that Ce^{3+} dissociates H_2O to give OH groups stable up to 600 K while chemisorbed H_2O desorbs by 300 K. Fig. 7 compares the adsorption of H_2O onto $CeO_2/Au(1\,1\,1)$ (Ce^{4+}), part A, and $CeO_{1.75}/Au(1\,1\,1)$ (Ce^{3+}/Ce^{4+}), part B, at 100 K with a series of sequential doses of H_2O (0.01–2.3 L). In Fig. 7A the lattice peak is present at 530.2 eV and a peak appears at 533.8 eV with increasing H_2O coverage. The position of this peak corresponds to H_2O ice layers on both $Au(1\,1\,1)$ [5] and $CeO_2(1\,1\,1)$ [10] and is very different to what occurs in the presence of Ce^{3+}. In Fig. 7B, the first peak to appear is located at 532.3 eV and is likely to involve contributions from OH groups and chemisorbed H_2O as reported by Kundakovic et al. [6]. Increasing the coverage of H_2O on the $CeO_{1.75}/Au(1\,1\,1)$ shows that the 532.3 eV peak saturates at 0.07 L and a peak at 533.8 eV appears corresponding to H_2O ice. H_2O does not dissociate on $Au(1\,1\,1)$ except in the presence of chemisorbed oxygen [5] so we can attribute the formation of OH exclusively to CeO_x.

Fig. 8 displays the effect of annealing both surfaces of Fig. 7 to 300 K. At this temperature it is reported that physisorbed multilayers of ice (533.8 eV) and chemisorbed H_2O have desorbed leaving

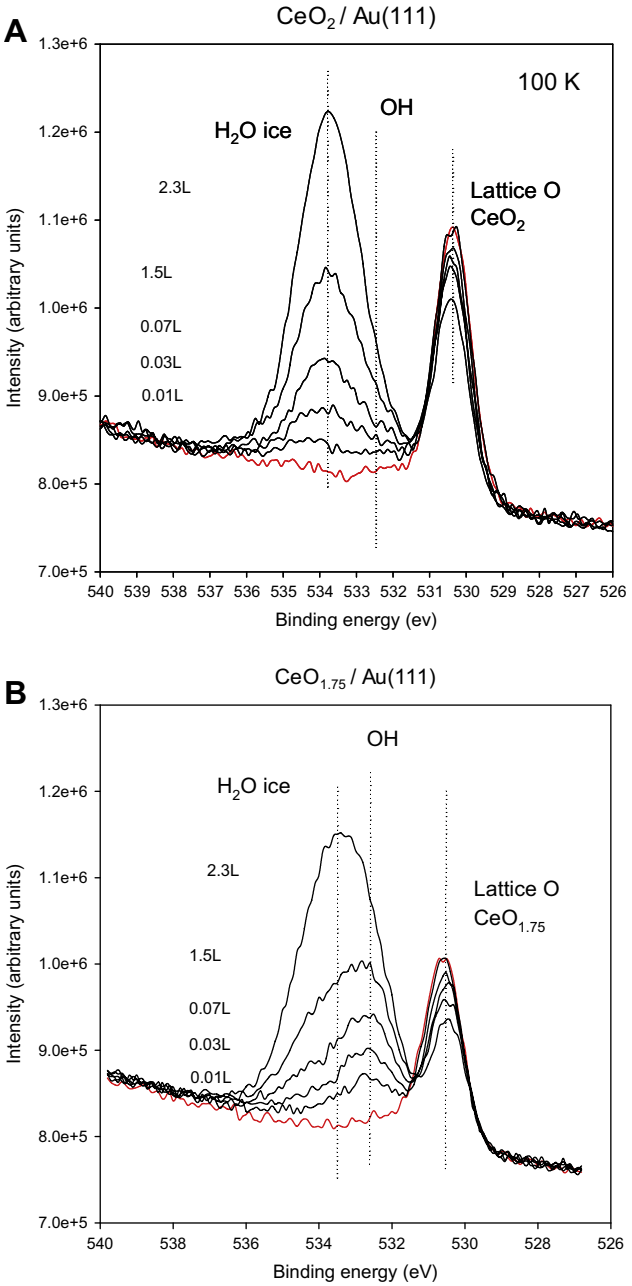

Fig. 7. sXPS spectra in the O1s region for sequential H_2O adsorption (0.01–2.3 L) onto $CeO_x/Au(1\,1\,1)$ surfaces at 100 K followed by annealing to 125 K. (A) $CeO_2/Au(1\,1\,1)$ and (B) $CeO_{1.75}/Au(1\,1\,1)$.

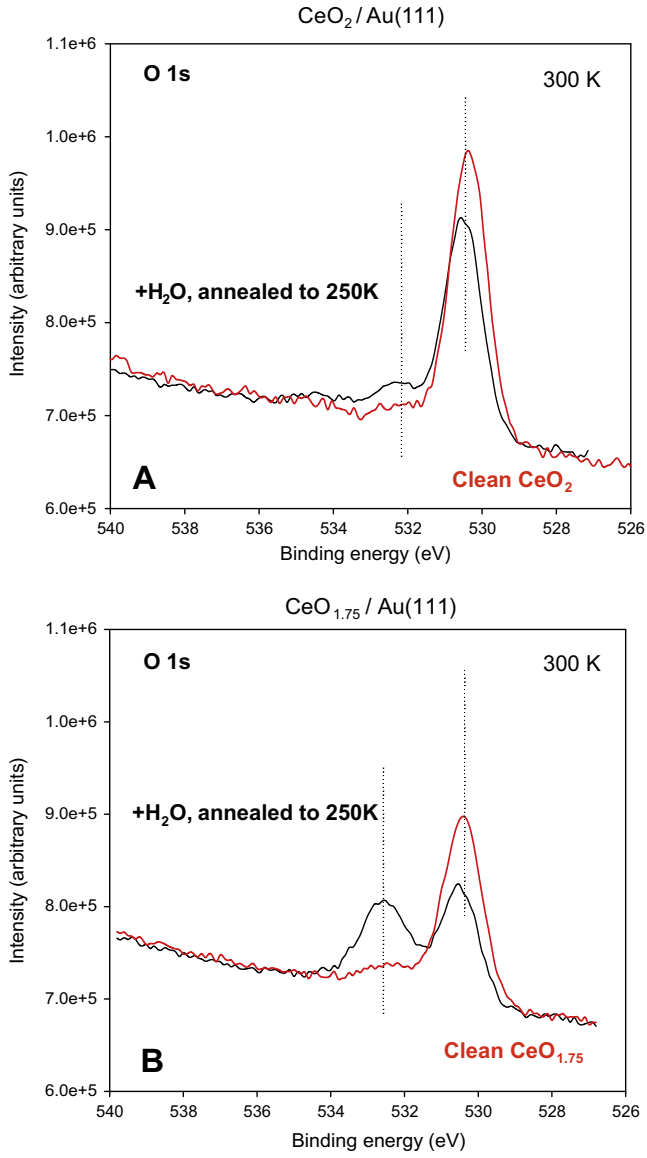

Fig. 8. sXPS spectra in the O1s region for H_2O (2.3 L) adsorption at 100 K on (A) $CeO_2/Au(1\,1\,1)$ and (B) $CeO_{1.75}/Au(1\,1\,1)$ surfaces followed by annealing to 300 K. The corresponding spectra for clean surfaces are shown as red traces. (For interpretation of the references to color in this figure legend, the reader is referred to the web version of this article.)

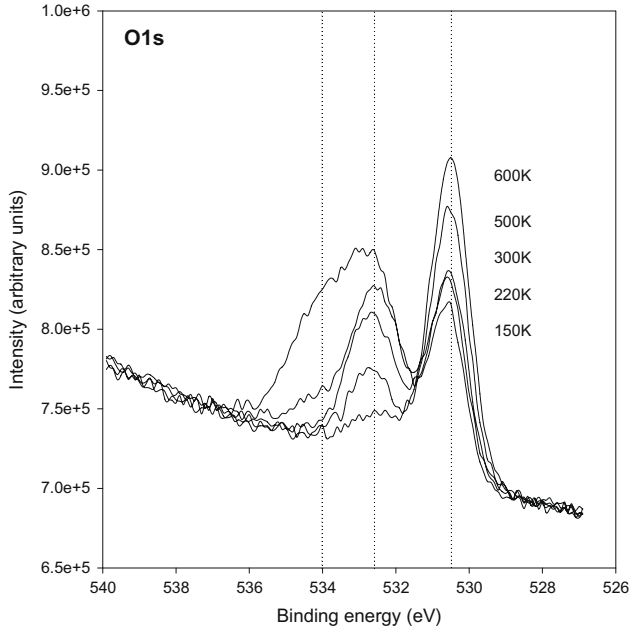

Fig. 9. sXPS spectra in the O1s region for a dose of 2.3 L of H_2O to $CeO_{1.75}$/Au(1 1 1) followed by annealing steps as depicted from 150 to 600 K.

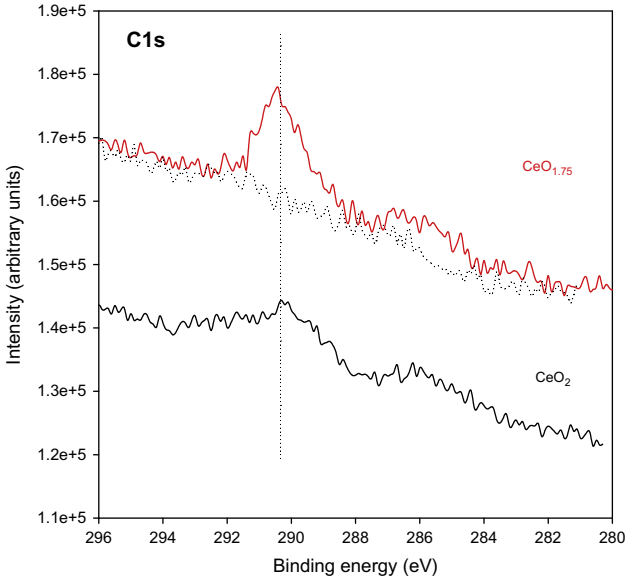

Fig. 10. C1s spectra of CO (3 L) exposed onto hydroxylated $CeO_{1.75}$/Au(1 1 1) and CeO_2/Au(1 1 1) at 100 K.

only the OH groups adsorbed (532.3 eV) on both surfaces. It is evident that the concentration of OH on the surface is proportional to the amount of Ce^{3+} present. Fig. 9 shows the effect of annealing the OH containing surface, $CeO_{1.75}$/Au(1 1 1), from 150 to 600 K. The OH peak at 532.3 eV appears to survive on the surface up to 600 K, and the reactivity pathway can be summarized on the CeO_2 and $CeO_{1.75}$ surfaces as follows:

$$[Ce^{4+}] \quad H_2O + O\ (\text{oxide}) \rightarrow H_2O\ (a) + O\ (\text{oxide})$$
$$H_2O\ (a) \rightarrow H_2O, \quad \sim 180\ \text{K}\ [6]$$
$$[Ce^{3+}/Ce^{4+}] \quad 2H_2O + \{O + \text{Vac}\}\ (\text{oxide}) \rightarrow 2OH\ (a) + H_2O\ (a)$$
$$H_2O\ (a) \rightarrow H_2O, \quad < 300\ \text{K}\ [6]$$
$$2OH\ (a) \rightarrow H_2 + 2O\ (\text{oxide}), \quad \sim 600\ \text{K}\ [6]$$
$$2OH\ (a) \rightarrow H_2O + O\ (\text{oxide})$$

3.5. Reaction of CO with OH/CeO_x/Au(1 1 1)

CO is reported to only interact weakly with CeO_2(1 1 1) and Au(1 1 1) [15,22,23]. Dissociation of CO was observed in the presence of M/$CeO_{1.75}$(1 1 1), where M = Rh [24,25], Pd [26], and Pt [27], but not for adsorption of the molecule on Au/$CeO_{1.98}$(1 1 1) [15]. Furthermore, DF calculations have pointed to a weak interaction between CO and the CeO_2(1 1 1) surface (E_{bind} 4.6 kcal/mol) but stronger interaction with the (1 1 0) surface (E_{bind} > 46 kcal/mol) resulting in carbonate formation [28]. In general, the coadsorption of CO and water can lead to attractive or repulsive interactions depending on the morphology or chemical nature of the surface [29]. Mullins et al. explored the reaction of CO + H_2O on CeO_2(1 1 1) films and found no noticeable reactivity except in the presence of Rh nanoparticles: CO dissociated on Rh while the H_2O dissociated on CeO_2 [6]. The spectroscopic data pointed to OH formation on $CeO_{1.75}$ and C on Rh, but no formates or carbonates were reported as a result of the CO + OH reaction.

Here, CO (3 L) was dosed onto hydroxylated ceria–gold surfaces with both oxidized CeO_2 and reduced $CeO_{1.75}$ stoichiometries. The hydroxyls were obtained by dosing 2.3 L of H_2O onto the cool surfaces followed by annealing to 300 K as discussed in the previous section. Fig. 10 shows the result of this experiment in the C1s region for both CeO_2 and $CeO_{1.75}$. A single peak at 290.2 eV and a broad feature at 286 eV appear on both surfaces with 3 L of CO exposure at 100 K. The intermediate on the $CeO_{1.75}$ surface shows a stronger contribution than on CeO_2. The 286 eV peak is likely to be traces of CO condensed on the surface. The 290.2 eV could be one of several potential intermediates (formates or carbonates) described above or the satellite features that arise from CO on Au(1 1 1) [5], hence making a conclusive identification difficult. The O1s region (not shown here) also has very similar fingerprints for CO, carbonates, and formates and the result is difficult to interpret convincingly.

Unlike the sXPS results, the NEXAFS provided additional insights. As discussed above and shown in Table 1, adsorbed carbonate and formate have distinctive features in the C K - edge region. Figs. 11 and 12 display the C K - edge for 3 L of CO on hydroxylated surfaces of CeO_2 and $CeO_{1.75}$, respectively. In Fig. 11, the grazing incidence (65°) shows contributions of two narrow peaks at 287.4 and 290.5 eV. The normal (0°) incidence shows a single narrow peak at 290.6 eV and a broader peak at 300 eV. This spectra has very similar appearance to that of Fig. 6 of CO_3 formation on CeO_x/Au(1 1 1). The 290.5 and 290.6 eV peaks can be attributed to the π^*C–O resonance with near equivalent contribution in both normal and grazing incidence and the broader peak at 300 eV to a weak σ_1^*C–O resonance. The 287.4 eV is also evident in Fig. 6 and maybe a contribution of CO molecularly adsorbed on the surface or likely to be the effect of beam damage of the surface species. It is evident that there is not a very strong interaction between the CO and the OH on the surface of CeO_2/Au(1 1 1). The formation of CO_3 shows that the CO prefers to bind to the surface oxygen and does not react with OH present at the small concentration.

Fig. 12 shows data for the exposure of 3 L of CO onto the heavily hydroxylated surface with a larger Ce^{3+} concentration. This set of C K - edge data is more complex than that of Fig. 11 with many contributions evident. The peaks that appear at 288 and 288.4 eV share close resemblance to that of the π^*C=O resonance in the grazing and normal incidence for formates as depicted in Fig. 3. The 290.4 and 290.3 eV peaks are close to the π^*C–O resonance of carbonates in Fig. 6 in the grazing and normal incidences. The peak at 286.1 eV is due to CO adsorbed on the surface. Weaker, broader contributions at 301.5 and 303.6 eV are likely a mixture of σ features from both the carbonate (CO_3) and the formate

Table 1
Major features in NEXAFS spectra of adsorbed HCOO and CO_3.

	$\pi^*C{=}O$	σ^*CH	$\sigma_1^*C{-}O$	$\sigma_2^*C{-}O$	$\pi^*C{-}O$	$\sigma^*C{-}O$
HCOO/Ag(1 1 0) [30]	288.3	292.2	298.6	301.9		
HCOO/CeO_2(1 1 1) [11]	288.1	290.9	298.5	300.8		
HCOO/CeO_x/Au(1 1 1)	288	290.6	299.4	301.7		
CO_3/Ag(1 1 0) [31]					290.1	~300.5
CO_3/CeO_2(1 1 1) [11]					290.5	~301
CO_3/CeO_x(1 1 1)/Au(1 1 1)					290.7	~300–302

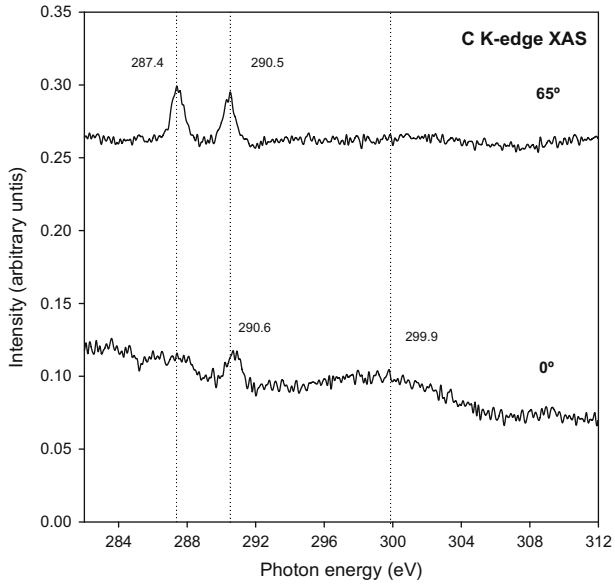

Fig. 11. C K - edge NEXAFS of CO (3 L) dosed to hydroxylated CeO_2/Au(1 1 1) at 100 K. Both the normal incidence (0°) angle and the grazing incidence (65°) spectra are presented here.

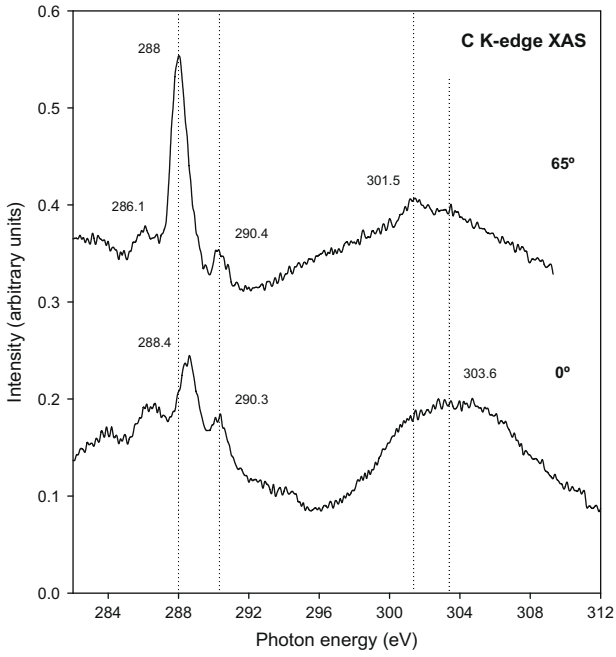

Fig. 12. C K - edge NEXAFS of CO (3 L) dosed to hydroxylated $CeO_{1.75}$/Au(1 1 1) at 100 K. Both the normal incidence (0°) angle and the grazing incidence (65°) spectra are presented here.

(HCOO) contributions. A possible scenario for reaction of CO with O in presence of OH is:

$$[Ce^{4+}] \quad 2CO + 0.5OH(a) + 2O(a) \rightarrow CO(a) + CO_3(a) + 0.5OH(a)$$
$$CO(a) + CO_3(a) + 0.5OH(a) \rightarrow 2CO_2 + 0.25H_2 + 0.5O(a)$$
$$[Ce^{3+}/Ce^{4+}] \quad 2CO + OH(a) + O(a) \rightarrow 0.5CO_3(a) + HCO_2(a) + 0.5CO(a)$$
$$0.5CO_3(a) + HCO_2(a) + 0.5CO(a) \rightarrow 2CO_2 + 0.5H_2$$

The coadsorption of H_2O and CO has been reviewed previously [29] with many examples therein of attractive and repulsive interactions between the two adsorbates on numerous metal surfaces, but no published study has demonstrated a strong interaction on oxide surfaces in UHV conditions. One study showed that on NiO(1 0 0), OH groups were 'blocking' adsorption sites and inhibiting the ability of CO to stick to that surface [32]. The CO + OH interaction in our study shows a distinct result, on a system that has a very strong reaction with H_2O for the formation of stable hydroxyls ($T_{desorption}$ = 600 K); a behavior that is unique to CeO_x/Au(1 1 1) and not seen on O/Au(1 1 1) or typical metal surfaces. The ratio of OH:O(oxide) on the surface dictates the chemical specificity of the intermediate that arises. In any case, one can speculate of a direct link of the CO + OH interaction to the WGS activity of CeO_x/Au(1 1 1). The addition of ceria nanoparticles to Au(1 1 1) is essential to generate an active WGS catalyst and to increase the production and stability of key reaction intermediates (OH, HCOO and CO_3). This is consistent with previous studies which show that ceria plays an active role in the WGS process [2,4,33,34].

The production of CO_3 by the reaction of CO with O sites of the oxide is expected when the OH groups are only a minor surface species. Very weak carbonate formation from the interaction of CO with a CeO_2(1 1 1) film has been previously reported by Mullins et al. [22] and visible in the C1s region at 290 eV. The HCOO formation is driven by the CO + OH reaction and an increase in the OH:O(oxide) ratio. It is also worth noting that the ability to inhibit the desorption of H_2O by recombination of OH and surface oxygen at lower temperature is also very important to the stability of the resulting intermediate. In terms of the reported WGS activity at higher temperatures (573–650 K), it is clear from this study that the Ce^{3+} is critical to OH formation and a likely scenario may be that the OH could spill over from the CeO_x nanoparticles on to the Au(1 1 1) surface. The same path may also yield stable HCOO ($T_{desorption}$ = 600 K) on the surface. Senanayake et al. [10] did report the stability of formates on both oxidized (Ce^{4+}) and reduced (Ce^{3+}) surfaces. The path to CO_3 formation, however, is less dependent on Ce^{3+} and as the intermediate is only stable up to 300 K and allows for CO_2 and H_2 to desorb freely, hence not a likely poison for the high temperature WGS.

The low-temperature (80–120 K) WGS as observed on O/Au(1 1 1) is very different in comparison [5]. It is clear that the Au(1 1 1) substrate alone plays only a minor role when the reaction takes place. The ability to dissociate water and stabilize OH over O/Au(1 1 1) is considerably weaker in comparison with CeO_x/Au(1 1 1). The formation of either CO_3 or HCOO species on the O/Au(1 1 1) surface probably poisons the low-temperature WGS reaction because both intermediates are too stable for allowing the for-

mation of CO_2 and H_2 below 120 K. The carboxylate (HOCO) intermediate is experimentally elusive and not seen in this work but remains a potential candidate in both the low- and high-temperature pathways for the water–gas shift reaction [4]. The low thermal stability of the carboxylate makes it an ideal transient species for the WGS and it may only be observed under steady-state conditions.

4. Conclusions

This work provides insights into the reaction pathways for the water–gas shift on an inverse CeO_x/Au(1 1 1) catalyst. The CeO_x/Au(1 1 1) system is considerably more active toward the high temperature (575–650 K) WGS than Cu/ZnO(0 0 0 $\bar{1}$), Cu(1 0 0) and Cu(1 1 1) surfaces. Post-reaction characterization of the CeO_x/Au(1 1 1) catalyst showed a small signal for adsorbed CO_x groups with a C1s binding energy of 289.6–289.9 eV. This binding energy matches well with those found for formate and carbonate groups bonded to CeO_x/Au(1 1 1). After examining the adsorption of HCOOH and CO_2 we found that formates and carbonates are stable species on CeO_x/Au(1 1 1) surfaces, with the former showing the greater thermal stability. H_2O dissociates readily in the presence of Ce^{3+} and forms hydroxyls that remain on the surface right up to the WGS reaction temperature (600 K). We present evidence that CO interacts with OH groups on an oxidized CeO_2/Au(1 1 1) surface by forming predominantly carbonates and on the reduced $CeO_{1.75}$/Au(1 1 1) surface to give both carbonates and formates. The carboxylates remain undetectable under UHV conditions but they cannot be ruled out as possible intermediates of the high-temperature WGS reaction on CeO_x/Au(1 1 1). The addition of ceria nanoparticles to Au(1 1 1) is essential to generate an active WGS catalyst and to increase the production and stability of key reaction intermediates (OH, HCOO and CO_3).

Acknowledgments

The work performed at BNL was supported by the US Department of Energy, Office of Basic Energy Sciences, under Contract DE-AC02-98CH10886. J.E. and M.P. are grateful to INTEVEP and IDB for partial support of the work carried out at the UCV.

References

[1] R. Kothari, D. Buddhi, R.L. Sawhney, Int. J. Global Energy Issues 21 (2004) 154.
[2] Q. Fu, H. Saltsburg, M. Flytzani-Stephanopoulos, Science 301 (2003) 935;
R. Si, M. Flytzani-Stephanopoulos, Angew. Chem. Int. Ed. 47 (2008) 2884.
[3] H. Idriss, Platinum Metals Rev. 48 (2004) 105;
C. Diagne, H. Idriss, A. Kiennemann, Catal. Commun. 3 (2002) 565.
[4] J.A. Rodriguez, S. Ma, P. Liu, J. Hrbek, J. Evans, M. Perez, Science 318 (2007) 1757;
J.A. Rodriguez, J. Hrbek, Surf. Sci. 604 (2010) 241.
[5] S.D. Senanayake, D. Stacchiola, P. Liu, C.B. Mullins, J. Hrbek, J.A. Rodriguez, J. Phys. Chem. C 113 (2009) 19536.
[6] L. Kundakovic, D.R. Mullins, S.H. Overbury, Surf. Sci. 457 (2000) 51.
[7] F.C. Meunier, D. Tibiletti, A. Goguet, S. Shekhtman, C. Hardacre, R. Burch, Catal. Today 126 (2007) 143.
[8] S. Hilaire, X. Wang, T. Luo, R.J. Gorte, J. Wagner, Appl. Catal. A: Gen. 258 (2004) 271.
[9] R.A. Ojifinni, N.S. Froemming, J. Gong, M. Pan, T.S. Kim, J.M. White, G. Henkelman, C.B. Mullins, J. Am. Chem. Soc. 130 (2008) 6801.
[10] S.D. Senanayake, D.R. Mullins, J. Phys. Chem. C 112 (2009) 9744.
[11] S. Ma, X. Zhao, J.A. Rodriguez, J. Hrbek, J. Phys. Chem. C 111 (2007) 3685.
[12] S.G. Ma, J.A. Rodriguez, J. Hrbek, Surf. Sci. 602 (2008) 3272.
[13] J. Nakamura, J.M. Campbell, C.T. Campbell, J. Chem. Soc. Faraday Trans. 86 (1990) 2725.
[14] P. Liu, J.A. Rodriguez, J. Chem. Phys. 126 (2007) 164705.
[15] J.A. Rodriguez, P. Liu, J. Hrbek, J. Evans, M. Perez, Angew. Chem. Int. Ed. 46 (2007) 1329.
[16] J.A. Rodriguez, J. Graciani, J. Evans, J.B. Park, F. Yang, D. Stacchiola, S.D. Senanayake, S. Ma, M. Perez, P. Liu, J.F. Sanz, J. Hrbek, Angew. Chem. Int. Ed. 48 (2009) 8047.
[17] C.V. Ovensen, P. Stoltze, J.K. Nørskov, C.T. Campbell, J. Catal. 134 (1992) 445.
[18] X. Wang, J.A. Rodriguez, J.C. Hanson, M. Perez, J. Evans, J. Chem. Phys. 123 (2005) 221.
[19] R. Burch, Phys. Chem. Chem. Phys. 8 (2006) 5483.
[20] J. Stubenrauch, E. Brosha, J.M. Vohs, Catal. Today 28 (1996) 431.
[21] X. Zhao, S. Ma, J. Hrbek, J.A. Rodriguez, Surf. Sci. 601 (2007) 2445.
[22] J. Hrbek, F.M. Hoffman, J.B. Park, P. Liu, D. Stacchiola, Y.S. Hoo, S. Ma, A. Nambu, J.A. Rodriguez, M.G. White, J. Am. Chem. Soc. 130 (2008) 17272.
[23] M.S. Pierce, K.-C. Chang, D.C. Hennessy, V. Komanicky, A. Menzel, H. You, J. Phys. Chem. C 112 (2008) 2231.
[24] D.R. Mullins, S.H. Overbury, J. Catal. 188 (1999) 340.
[25] J. Stubenrauch, J.M. Vohs, J. Catal. 159 (1996) 50.
[26] S.D. Senanayake, J. Zhou, A.P. Baddorf, D.R. Mullins, Surf. Sci. 601 (2007) 3215.
[27] D.R. Mullins, K.Z. Zhang, Surf. Sci. 513 (2002) 163.
[28] M. Huang, S. Fabris, J. Phys. Chem. C 112 (2008) 8643.
[29] M.A. Henderson, Surf. Sci. Rep. 46 (2002) 1.
[30] P.A. Stevens, R.J. Madix, J. Stohr, Surf. Sci. 230 (1990) 1.
[31] R.J. Madix, J.L. Solomon, J. Stohr, Surf. Sci. 197 (1988) L253.
[32] H.E. Sanders, P. Gardner, D.A. King, M.A. Morris, Surf. Sci. 304 (1994) 159.
[33] J.B. Park, J. Graciani, J. Evans, D. Stacchiola, S. Ma, P. Liu, A. Nambu, J.F. Sanz, J. Hrbek, J.A. Rodriguez, PNAS 106 (2009) 4975.
[34] I.D. Gonzalez, R.M. Navarro, W. Wen, N. Marinkovic, J.A. Rodríguez, F. Rosa, J.L.G. Fierro, Catal. Today 149 (2010) 372.